

# THE MODELLING OF CAUSTICS TO PRODUCE A PROJECTION IMAGE

Luke Maguire<sup>a</sup>, Marios Papas<sup>b</sup>, Wojciech Jarosz<sup>c,b</sup>, Phillip Fox<sup>a</sup>, Greg Dicoski<sup>a</sup>, and  
Maria Olivares<sup>b</sup>

<sup>a</sup>Note Issue Department, Reserve Bank of Australia, Craigieburn, Victoria, Australia

<sup>b</sup>Disney Research, Zurich, Switzerland

<sup>c</sup>Dartmouth College, Hanover, NH, USA

## 1. ABSTRACT

The Projection-Based Image is a new banknote security feature that projects a desired image when an array of microlenses embossed into the banknote substrate is exposed to a light source. The feature is designed computationally to make the projected image difficult to discern by inspection of the lens structures, and to accommodate a range of light sources, allowing wide accessibility to users with a simple mobile phone flash. The projected image is formed from a collection of Gaussian-shaped caustic profiles, each arising due to light refracting through a single microlens.

**Keywords:** caustics, micro-optics, smartphone authentication, device assisted feature

## 2. INTRODUCTION

Device-assisted features are commonly included on banknotes to provide an added layer of surety to users not confident of the authenticity of overt features on the banknote. These features are not immediately visible to the user, but with the use of a simple tool can provide an immediately obvious and describable effect that can be used by cash handlers and the public.

The most commonly used second-level feature is fluorescent or phosphorescent ink. While the widespread availability of UV lamps has made fluorescent inks popular as a retailer-level security feature, the inks are now widely available for purchase, reducing their efficacy against counterfeiting. Many alternatives have been proposed with the aim of matching the accessibility and ease of use of fluorescent features, while offering a similar perceived level of security. However, these schemes often require either specific tools to authenticate, such as polarisers for liquid crystal features. Diffractive optical elements (DOEs), another feature in common use, require illumination with a laser pointer to confirm authenticity, and although they can be viewed with a point light source, many users find the effect difficult to understand or are unable to see the diffractive image.

Smartphones have been proposed as the ideal tool for authenticating banknotes, given their rapid uptake by communities worldwide; in 2016, 84% of Australians owned a smartphone, including 94% of people under the age of 25<sup>1</sup>. A number of schemes have been proposed to utilise this easy access to smartphones for authenticating banknotes<sup>2,3</sup>, including schemes aimed at the vision impaired community<sup>4</sup>. However, the majority of these require downloading of a specific app to authenticate an embedded print design, signal or feature. This presents a barrier to their use; if a user does not have the tool immediately accessible at their time of need, they are unlikely to make use of this means of authentication.



*Figure 1: The PBI feature. The lens array, applied to polymer substrate is illuminated by an iPhone 6s flash. The projected image can be clearly resolved.*

This paper presents a new security feature that utilises easily accessible functionality, available on all smartphones, as the authentication tool. The Projection-Based Image (PBI), shown in Figure 1, is an array of microlenses embedded in the window of a polymer banknote that projects a high-contrast image when illuminated by a smartphone flashlight. The feature can be applied directly to polymer film in a single process using established banknote production techniques; that is, no additional print processes are required. The optical effect is straightforward to explain to the public, and the projected image can be easily observed even by untrained users. The flashlight function is accessible from the lock screens of both Apple and Android phones in their standard configurations, so the tool required to use the feature is immediately at hand. However, the PBI is not limited to smartphone use, as any bright point light source will project the image. The sun, as shown in Figure 2, projects an image of high clarity at a short projection distance.

The feature is based on a system, described in the paper of Papas *et al*<sup>5</sup>, for designing surfaces to generate custom caustic images when illuminated by a light source. Caustics are the envelopes of light rays produced by refraction or reflection of light from a curved or complex surface<sup>6</sup>. The term also refers to the projection of the envelope of rays onto a surface, which are often observed in nature as the patterns produced by sunlight shining through rippling water onto the bottom of clear pools of water. The most commonplace example of designing reflective surfaces to

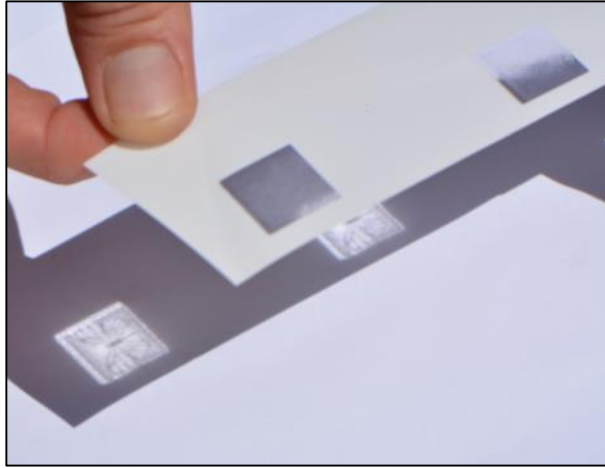


Figure 2: The PBI feature, illuminated by the sun.

produce a given caustic is the manufacture of lamp reflectors to create a desired radiance distribution for a fixed light source position, such as in certain spotlights<sup>7</sup>. The system developed by Papas et al was able to produce a design for an array of refractive lenses that can create a caustic that will project any chosen monochrome image onto a surface.

For this work, the method of Papas *et al* was extended to accommodate a number of banknote-specific constraints, which are detailed in Sections 3 and 4. In particular, this project showed that the method could be adapted to accommodate local light sources, explicit geometric constraints, such as overall surface thickness, and protective coatings. It also empirically provides de-correlation of the projected image and surface geometry. In contrast, more recent publications<sup>8,9</sup> in the field explicitly create smooth lens geometries, with no control over the surface geometry; in some cases the image is directly visible on the lens array.

### 3. CAUSTIC DESIGN

The algorithm developed by Papas et al was originally designed to produce lens surfaces as smooth as possible, so that the lens arrays could be milled into a PMMA plate by an automated engraver machine<sup>†</sup>. A prototype lens array produced using this algorithm is shown in Figure 3. The lens array is  $9 \times 9$  cm, consisting of  $32 \times 32$  individual

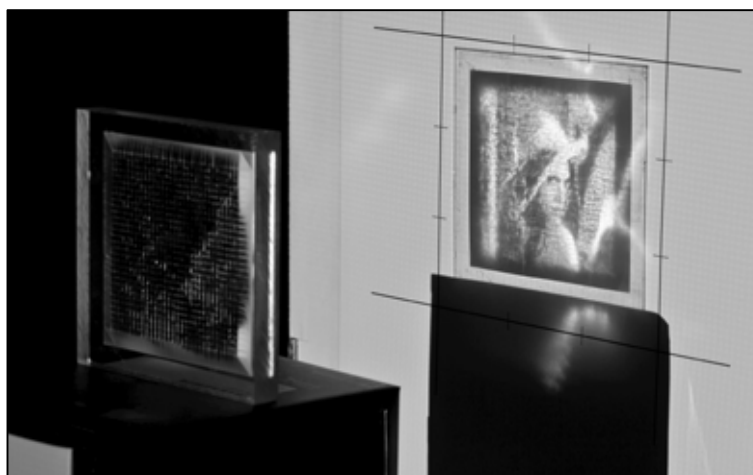


Figure 3: A large scale lens array projecting a caustic image

<sup>†</sup> A Roland DGA EGX-600 Engraver with a maximum cutting area of  $61 \times 40 \times 4.2$  cm, maximum software spatial resolution 0:01 mm, and a repeat accuracy of 0:05 mm was used. The engraver uses a C2-171-010K Carbide Tipped Engraving Cutter.

lenses. The array is illuminated by a white-light projector, approximating a distant collimated light source.

The following section describes the modified algorithm for producing lens arrays suitable for use on banknotes. Section 4 contains a discussion of the constraints that must be met to ensure the lens array is suitable for use on banknotes, and the modifications to the algorithm that were made to accommodate these results.

The presented method consists of three main steps, detailed in the following sections:

- Image Decomposition: decomposing the image into a set of anisotropic Gaussian kernels
- Microlens Design: design the shape of each microlens to project the assigned Gaussian kernel
- Microlens Arrangement: arrange microlenses to minimise the total lens thickness

### 3.1 Image Decomposition

The first step is to create an approximation of the target image that could be produced by the lens array. The lens surface consists of a grid of  $N_g = n \times n$  "Gaussian lenses" or microlenses; each microlens will be responsible for redirecting incident light through refraction into a Gaussian footprint. As the sum of these Gaussians will form the target image, the initial step takes the form of decomposing the desired image into a Gaussian mixture model. Each Gaussian in this model should integrate to a constant value, since the projected areas of the individual microlenses are approximately equal, so it is assumed that an approximately equivalent amount of light is incident on each microlens for redirection. With this constraint in place, the remaining parameters of the Gaussians are fitted using a standard Expectation Maximization (EM) optimization<sup>10</sup>. The starting point for EM is estimated using Capacity Constrained Voronoi Tessellation<sup>11</sup>, with isotropic Gaussians. The EM optimization is allowed to shift the centres, eccentricity, and orientation of the Gaussians, but not their total energy. Anisotropic Gaussian kernels align better than isotropic kernels to image features, and reduce the number of required Gaussians. The effect of varying the number of Gaussian kernels in the image decompositions is demonstrated in Figure 4.



Figure 4: Image decomposition into anisotropic Gaussians using Expectation Maximization and isotropic Gaussians using Capacity Constrained Voronoi Tessellation<sup>‡</sup>

<sup>‡</sup> Imagery supplied by Library of Congress - Oren Jack Turner/Science Faction/Getty Images

As noted earlier, the security feature version of the array will use a smartphone flash as the light source, which can be approximated by a disk-shaped light source. The blurring that will occur from such a light source is approximated by estimating the variance of the circle of confusion at the image plane, and subtracting it from the variance of each Gaussian. This method does not improve the result in cases where the Gaussian variance is smaller than the variance of the circle of confusion of the light source.

Given the Gaussian decomposition of the image into  $N_g$  Gaussian kernels, the next step is assigning a part of the lens surface (microlens) to each Gaussian, and then computing the shape of each microlens such that it will refract incident illumination to the assigned Gaussian-shaped irradiance distribution on the projection plane.

### 3.2 Microlens Design

The lens surface is composed out of rectangular microlenses, each responsible for projecting a Gaussian shaped irradiance distribution on the projection plane. To achieve the desired irradiance distribution each microlens is uniformly subdivided into microfacets, and each facet aimed towards a predetermined location of the Gaussian distribution. The mapping between centres of facets on the microlens and the Gaussian distribution on the image plane is performed using Gaussian warping. Once this mapping is completed for all facets of a microlens, the normal of each facet is estimated such that incident light will be refracted towards the desired target on the image plane. Finally, once all facet normals are computed, they are integrated into a continuous microlens surface using Poisson reconstruction by solving a linear system.

**Gaussian Warping:** The surface of the lens is subdivided into a grid with  $N_g$  microlenses, equal to the number of Gaussian kernels. Each Gaussian kernel is randomly assigned to a microlens on the lens surface. Given the position and the anisotropy of the assigned Gaussian on the projection plane, the shape of each smooth microlens is designed such that it will refract light with the assigned Gaussian distribution on the projection plane.

Initially, sample points are warped from the unit square to a unit disk by using Concentric Mapping, and then to a unit Gaussian by using a modified Box-Muller transform<sup>12</sup>. Figure 5 shows an example visualisation of warping from the unit square to the unit disk and then to the unit Gaussian. The Gaussian samples are then transformed to world space by first translating and scaling all the points according to the normalized image coordinate of the centre and variance of the Gaussian, and secondly by the applying the transformation matrix from the unit image to the desired position and scale on the image plane.

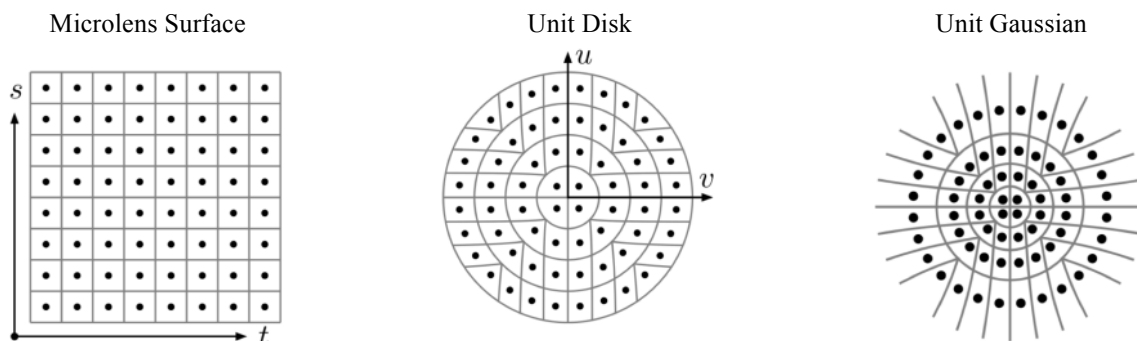


Figure 5: Warping a point distribution from unit square to a unit disk and finally to a unit Gaussian.

**Facet Normal Estimation:** Given an incident light direction  $\omega_i$  and an outgoing direction ( $\omega_o$ ) towards a point of the assigned Gaussian ( $T$ ), the surface normal  $\vec{n}_f$  at the centre of each facet is calculated (Figure 6). This uses the following formula, based on Snell's law of refraction, such that light originating from  $\omega_i$  will refract to  $T$ :

$$\vec{n}_f = f_n(\vec{\omega}_i \cos(\theta_i) + \vec{\omega}_x \sin(\theta_i))$$

where  $\theta_b = \arccos(-\vec{\omega}_i \cdot \vec{\omega}_o)$ ,  $\theta_i = \frac{-\arctan(\eta_{a|c} \sin(\theta_b))}{\eta_{a|c} \cos(\theta_b) - \eta_l}$ ,  $\vec{\omega}_x = f_n(f_n(\vec{\omega}_i \times \vec{\omega}_o) \times \vec{\omega}_i)$ ,  $f_n(\vec{x}) = \frac{\vec{x}}{\|\vec{x}\|_2}$ ,  $\|\vec{x}\|_2 \neq 0$

**External microlenses with collimated light:** In the case of distant collimated light, incident perpendicular to the flat back side of the lens, the back interface does not alter the incident direction and  $\vec{\omega}_i$  is equal to the normal of the back side  $\vec{n}_b$ .

**External microlenses with local light:** In the case of a local point light source the incident light direction will be altered by the back side of the lens. Unfortunately, there is no closed form solution for finding the incident light direction  $\vec{\omega}_i$  on the microlens and refraction point  $P_o$  given the location of the point light source and the distance to the back surface. The direction and refraction point were computed by employing a small number of iterations of a Newton-Raphson solver as described in Section 3.2 of Walter et al<sup>13</sup>.

**Enclosed microlenses with local light:** Finally, in the case where the microlens is coated with a dielectric material with a different index of refraction, the outgoing direction will also be altered by the refraction at a point  $P_o$  on the coating/air interface. Iterations of the Newton-Raphson solver are again employed to compute  $P_o$  and  $\vec{\omega}_o$ , such that when the outgoing light ray is refracted then it will end up in the desired location on the projection plane.

**Microlens geometry estimation:** Finally, the normals are integrated to generate the microlens geometry by using a Poisson reconstruction process. Experiments showed that, with a discretization of each microlens into  $M \times M = 21 \times 21$  facets, a high-quality Gaussian irradiance distribution on the image plane can be achieved.

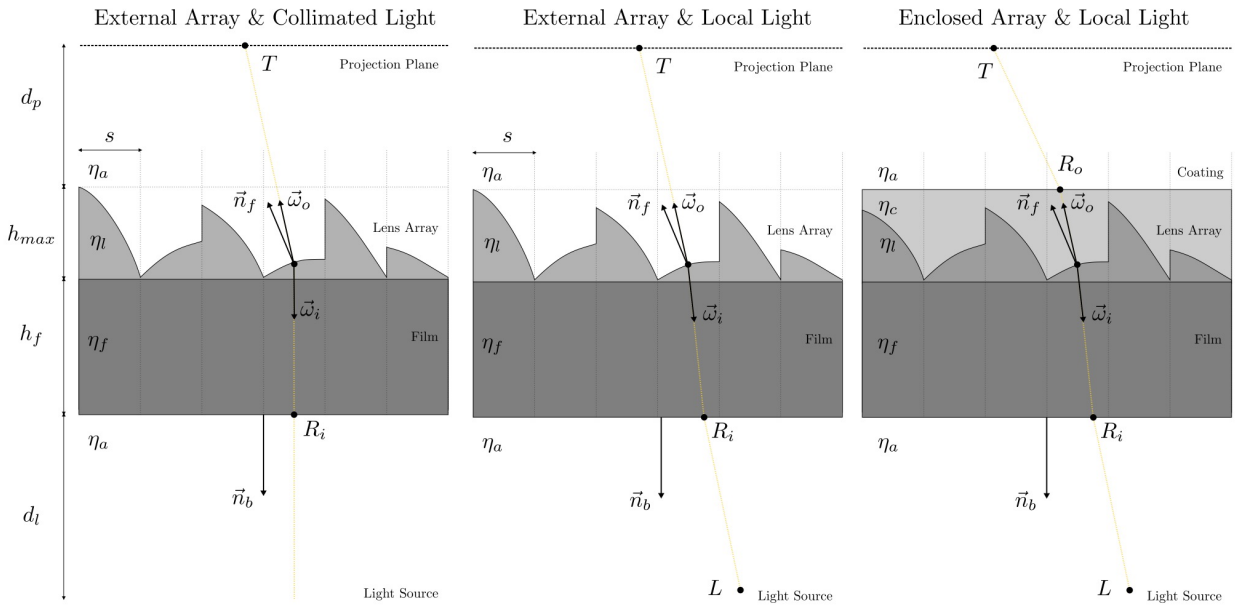


Figure 6: Schematics of lens array cases accommodated by the design algorithm

### 3.3 Microlens Arrangement

The microlenses are arranged utilizing a Simulated Annealing optimization<sup>14</sup>. Each microlens is initially randomly assigned to a Gaussian kernel. The optimization procedure then re-arranges and re-aims the microlenses by progressively decreasing the tilt of each microlens. The goal for this case is to minimize the overall thickness of the lens array, facilitating the fabrication of the PBI on banknotes.

Given a random assignment of microlenses to Gaussians, the microlens geometry is approximated with a planar facet that has its centre aimed towards the centre of the Gaussian. The normal of the approximate facet is calculated using the equations presented in Section 3.2. Given the normal, the height variation  $h_f$  of each facet is calculated by

$$h_f = s (|\vec{n}.x/\vec{n}.z| + |\vec{n}.y/\vec{n}.z|)$$

where  $s$  is the side length of the facet and  $\vec{n}.x$ ,  $\vec{n}.y$ ,  $\vec{n}.z$  are the x-, y- and z-axis components of the facet normal.

As the height of each facet is progressively computed, the height is stored with the microlens index in a sorted heap-type data structure in descending order with respect to height variation. This data structure allows efficient  $O(1)$  access on the height, index, and target of the microlens with the largest height variation ( $h_{max}$ ), and  $O(\log N)$  insertion and deletion times. The main loop of Simulated Annealing optimization will later query for the microlens with the largest height, and will change its target and direction with another microlens billions of times, so it is crucial to be able to perform these queries and changes as efficiently as possible.

Given the initialized heap generated from the random assignment of facets to Gaussian centres, thickness optimization can be started, with the goal of identifying an arrangement of facets that produces the smallest possible height variation  $h_{max}$ . In the spirit of the Simulated Annealing optimization, an upper bound threshold  $T$  is defined at each iteration, which limits the increase of the maximum height variation  $h_{max}$  for each swap. Within the iteration, a swap of targets between the facet with the maximum height variation  $h_{max}$  and another random facet is tested. The maximum height variation of the facets with the new targets  $h'_{max}$  is computed, and only if  $h'_{max} - h_{max} < T$  is the swap accepted and the updated heights inserted into the heap data structure; otherwise the swap is rejected. Each iteration concludes when the number of attempted swaps reaches  $N_i = 50 N_g$ , or after 2000 accepted swaps, where  $N_g$  is the number of microlenses. After each iteration concludes the acceptance threshold for the  $i$ th iteration is updated as follows:

$$T_i = T_0 \exp(-i/1000),$$

where  $i$  is the iteration index and  $T_0 = 0.02 h_{max}$  is the initial threshold, with  $h_{max}$  computed right after the initial random assignment of microlenses to Gaussians. As the optimization progresses, swaps that can predominantly improve the maximum height variation will be accepted. The optimisation will cease when, for a given threshold  $T_i$ , there are no acceptable swaps found or if the target thickness is achieved. The optimisation progression is illustrated in Figure 7. Once the optimization converges to a local minimum, each single facet microlens approximation is replaced with  $M \times M$  microfacets and the geometry of the microlens computed such that it will refract the assigned Gaussian distribution (Section 3.2).

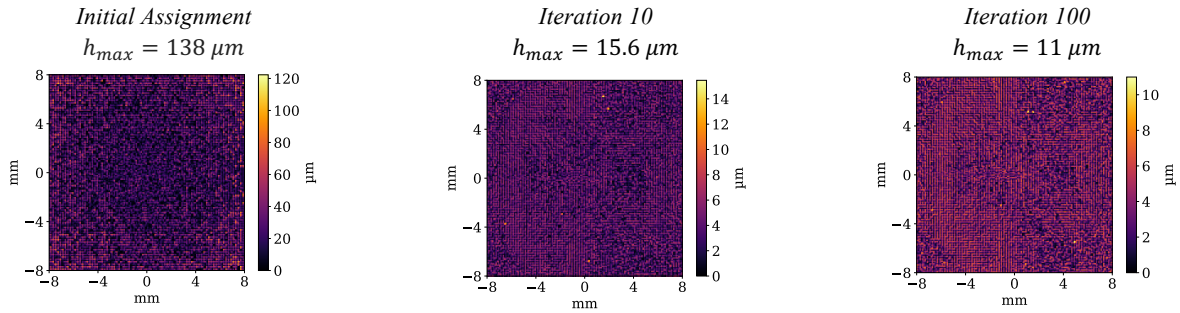


Figure 7: Progression of the Simulated Annealing optimization. The lens geometry is visualized as a height field at snapshots during the optimization.

#### 4. OPTIMIZATION FOR SECURITY FEATURES

The first implementation of the caustic algorithm used the freedom provided by the large, thick glass substrate, limited only by the resolution of the etching tool, to create caustic images from lens arrays with strong focusing power. It used the original algorithm by Papas et al, which solved the special case of microlenses illuminated by an ideal collimated light source. The key challenge for optimisation for banknotes was to ensure the same image quality could be re-produced at banknote scale, and using existing manufacturing processes.

The algorithm described in Section 3 extends the original algorithm to a general case for designing lens arrays, providing solutions for the cases where the light source is local, and for the case where the microlens is enclosed between two dielectric materials with different indices of refraction. This section details the design constraints that also had to be accommodated in the algorithm to ensure the lens arrays produced were suitable for banknote use.

**Manufacturability:** Polymer security features, such as CCL Secure’s Horizon™, have shown that relatively thick lenses can be integrated into banknote production without difficulty. Based on the RBA’s past experience with lens<sup>15</sup> and micro-optics features<sup>16</sup>, the height of the lens array was constrained to 15 μm. However, whereas the original arrays were 32 × 32 lenses in a 9 cm square, the fabrication method can accommodate 80 × 80 microlenses within a 16 mm square, allowing substantially improved resolution in the projected image.

As the original lens arrays were unconstrained by limits on thickness, the surface optimization process focused on producing a lens surface as smooth and continuous as possible for easy fabrication with a milling machine. For banknotes, the strict requirement on thickness is balanced against a fabrication method, detailed in Section 5 that allows discontinuities between lenses.

To meet the thickness requirement, the nature of the optimization and the error function were changed. Instead of optimizing for continuity between neighbouring microlenses a new error function is optimized that corresponds to the maximum height variation among all microlenses (i.e. tilt), or equivalently, the maximum thickness of the lenses. Implementing the new error function in a naïve manner within the simulated annealing optimization framework results in notoriously slow convergence rates. This arises because the simulated annealing optimization chooses two microlenses at random, attempts a swap of targets, and then evaluates the new value of the error function. If the error function change is less than a predefined threshold then the swap is accepted and the optimization progresses. The probability of changing the value of the error function in our scenario is equal to two over the number of microlenses. In all provided examples 80×80 = 6400 microlenses were used, which provides a good compromise between image quality and required manufacturing precision. The convergence was drastically

improved with the use of a novel heuristic that efficiently tracks a sorted list of the most tilted microlenses in descending order and changes the target of the most tilted microlens with another random microlens, such that each swap will provide a guaranteed change of this new error function.

For a lens array with 6400 microlenses, the total number of unique microlens arrangements that can generate the desired caustic is  $6400! \sim 2.34 \times 10^{21582}$ . The randomized simulated annealing optimization will stop at a local minimum and output a surface from a smaller subset which also satisfies the thickness constraint. It was empirically observed that the surface of the lens array is de-correlated from the projected image; i.e., the projected image cannot be seen on the lens array surface. Instead, all generated lens arrays exhibit a random noise appearance. This is attributed to the random nature of the simulated annealing algorithm, in conjunction with the large number of expected local minima which satisfy the thickness constraint.

**Adversarial resistance:** A straightforward means of increasing resistance against basic level counterfeiting is to ensure the projected image cannot be discerned from inspection of the lens array. This can be achieved by ensuring lenses that create bright areas of the projected image are distributed across the lens array.

Resistance against advanced level counterfeiting can be further enhanced by covering the lens with a protective layer to prevent casting of a mould from the lens array. The original method was limited to lenses with external microlenses on the front dielectric-to-air interface and a flat back side. For this project, the algorithm was extended to design a new lens geometry that allows for both sides of the lens to be flat by overlaying two materials with different indices of refraction and having the microlens surface enclosed in between.

**Ease of use:** Using smartphones as light sources makes the feature immediately accessible to the general public. The original method assumed collimated incident light from the flat back side of the lens, requiring calculation of refraction only at the microlens surfaces, saving the need to compute the distortion due to refraction at the back interface.

However, the light source-to-lens distance and lens-to-image plane distances must be constrained so that the user can hold both a light source and banknote easily to project the image. Constraints of 300 mm for light source-to-lens and 150 mm for lens-to-image plane were included in the algorithm.

## 5. FABRICATION

The PBI is designed to utilise the transparency of polymer banknotes. The design parameters listed in Section 4 create a feature suited to incorporation into a small window on the banknote, of the type included on Australian banknotes, although it can be incorporated into any clear window. The PBI is most suited to application on the polymer substrate through embossing the lens array into a UV-curable ink.

Embossing masters are created through a multi-step process. The first step is to produce a silica master of the lens array; the lenses are produced in the orientation they will appear on the banknote. A direct-write, maskless laser lithographic process is used to write the lens pattern directly into a resist coated on a silica wafer. The lens array is directly written into a photoresist of up to 20  $\mu\text{m}$  thickness using a UV laser. The energy output and defocus of the writing beam is continuously adjusted as the pattern is written, ensuring highly accurate replication of the lens array. While a number of micromachining techniques were investigated, this direct write lithographic process was the only technique capable of creating the optical quality of the lenses required within an industrially practical writing time.

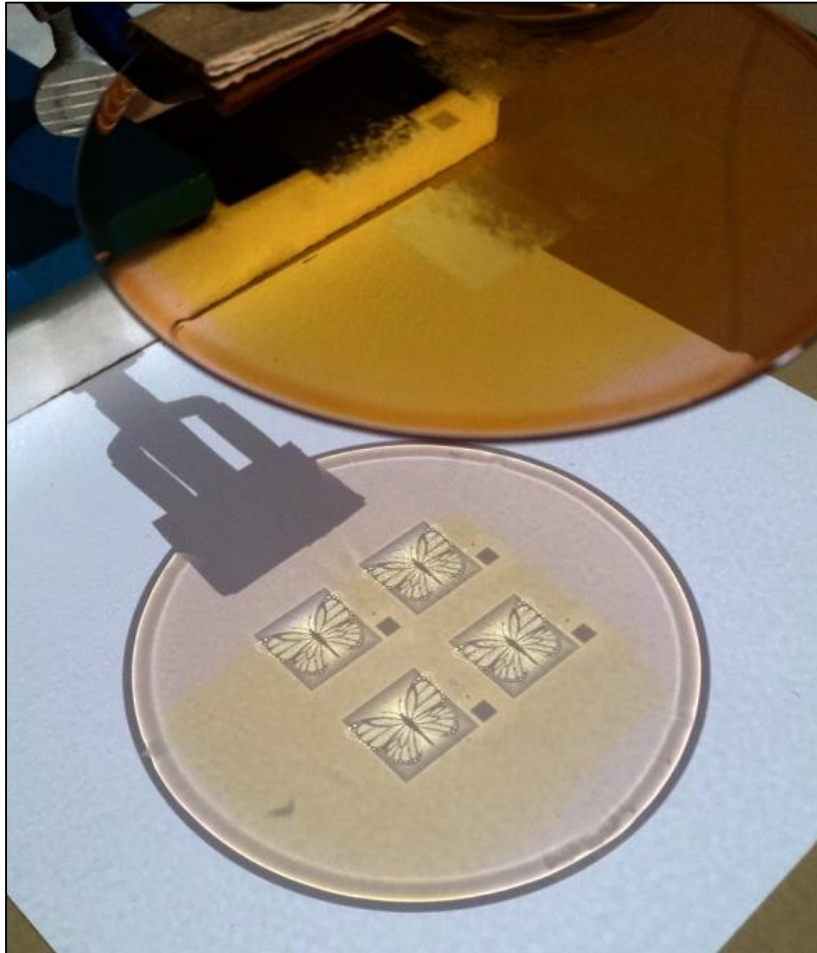


*Figure 8: Silica master containing four PBI lens arrays. The image projected from the lens arrays is also shown. A Samsung smartphone flash was used to project the image.*

The resist is then polymerised to produce a master, as shown in Figure 8. The depth of the engraving in the polymerised resist is closely calibrated to the laser energy absorbed at each point.

A nickel embossing shim is grown from the silica master. UV recombination processes are then used to produce a production-ready plate from this single shim.

Two production trials have been conducted on reel-to-reel presses, using UV-embossing to apply the feature to polypropylene film. The PBI was successfully applied on the film at typical production speeds (up to 90 m/min) used for similar lens features. A UV curable resin is applied at a thickness of 10 gsm to ensure defect-free replication. The thickness of this resin layer needs to be accurately controlled as the use of a thinner layer results in two issues: bubbles within lens elements and non-filling of lenses along lens boundaries. Both defects add noise to the projected image and reduce efficacy. However, correct setting of initial press conditions ensures these defects do not develop during production. All lens arrays measured have been below 15  $\mu\text{m}$  thick, a requirement for inclusion of the feature of the banknotes.

## **6. RESULTS**

### **6.1 Generation of lens arrays**

Prior to fabrication, simulations were conducted to ensure the constraints detailed in Section 5 could be met when designing for an arbitrary image. Figure 9 shows a generated lens array designed to project the target butterfly

image, and a simulation of the caustic image that would be projected from this lens array<sup>§</sup>. In all examples, the disk light source ( $\varnothing$  2.5mm) is placed at a distance of 300mm from the back side of the lens and the projection plane is located at 150mm from the front. As can be observed, the lens array fits within the thickness constraint of 15  $\mu\text{m}$ . The simulated caustic image is slightly less resolved than the target image. As shown in Figure 4, the resolution could be improved with a higher lens density. However, this is likely to have other detrimental effects on the lens array, including introduction of noise into the image through scattering and potentially diffraction from the boundaries between individual lenses. The strong agreement between the simulated and target images was sufficient justification to warrant fabrication of an embossing master for the feature.

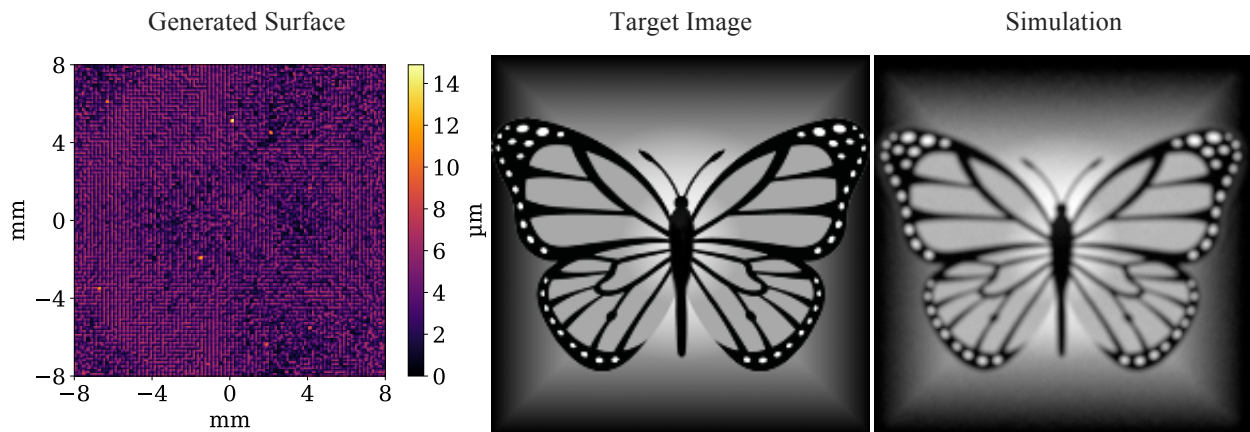


Figure 9: For the target butterfly image shown in the middle, a generated lens surface is shown on the left, and simulated projected image on the right.

## 6.2 Replication of lenses

As described in Section 5, lens arrays were produced on polypropylene film using a reel-to-reel UV embossing process. Figure 10 shows a comparison between the simulated projected image and the image projected from a PBI sample using the flashlight from a Google Nexus 4 mobile phone as the light source. The sample chosen does not have any opacifying layers applied to the film, which may assist framing of the image and would reduce background noise.

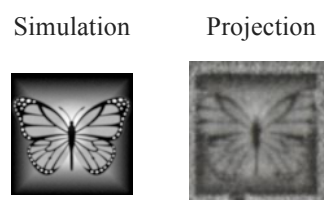


Figure 10: Comparison of simulated and actual projected images (actual size).

Analysis of the embossed lens arrays was conducted using a Bruker Contour GT-K 3D Optical Microscope to record the height of the embossed lens arrays. Height readings were taken at 4  $\mu\text{m}$  intervals across the width of the lens array, and the recorded profile was processed to remove low frequency noise arising from the measurement process. A comparison between the designed and manufactured lens arrays is shown in Figure 11.

<sup>§</sup> The simulation is rendered using the particle tracer integrator of Mitsuba, an open source physically-based renderer.

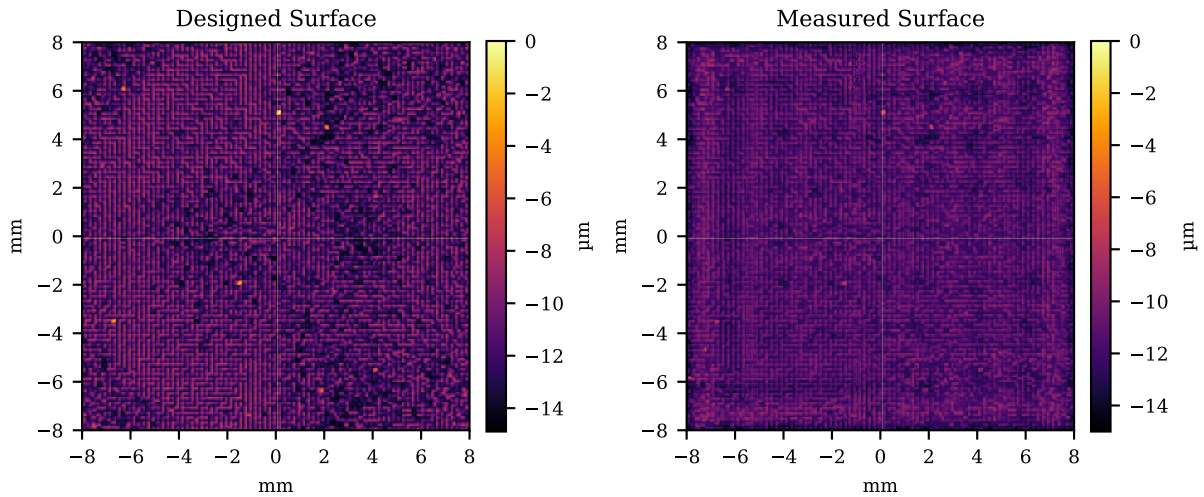


Figure 11: Comparison of designed lens array and measurement of UV-embossed lens array.

Figure 11 shows that the measured and designed arrays have the same height envelope; the thickness constraint included in the lens design was met in the manufactured array. However, agreement between the design and fabricated arrays is not immediately obvious. Figure 12 shows line plots of the designed and measured arrays, taken in both the x- and y-directions. The profiles are taken at  $x = 0.07$  mm and  $y = 0.07$  mm; that is, 1 mm from the top and right edges of the arrays.

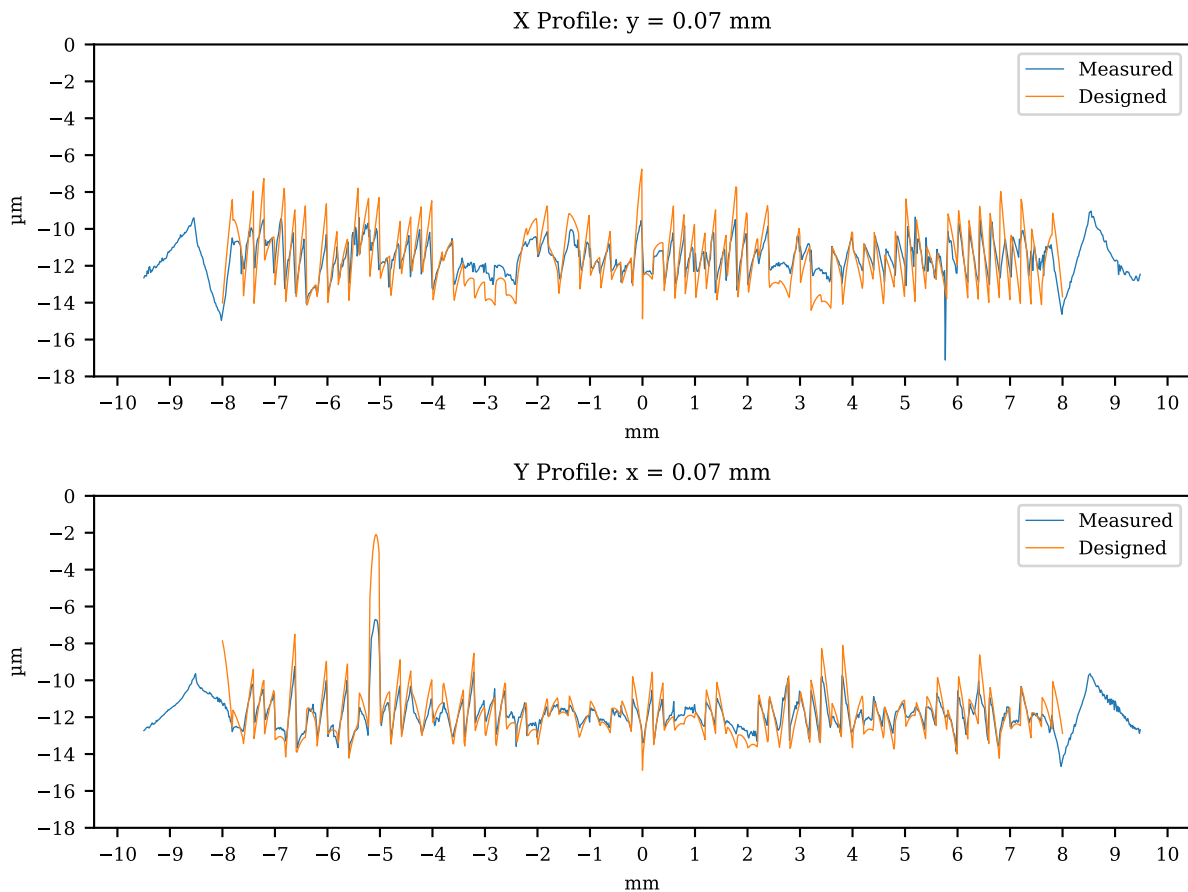


Figure 12: Line profiles of designed and measured lens arrays

Figure 12 shows broad agreement between the measured and designed lens, but a number of differences are also apparent. In particular, it can be seen that the measured array does not replicate some of the highest and lowest

points of the lens array. This is due to a manual “smoothing” across the edges of adjacent lens elements, aimed to reduce the steepness of the transition. The smoothing algorithm was implemented to facilitate the replication of lens arrays during the platemaking process. These adjustments were made after the lens array was designed; in future, this smoothing will be incorporated into the design algorithm. The shallow ramps at each of the measured profile were also added to facilitate the fabrication of embossing shims.

While there is not perfect agreement between the designed and measured profiles, the quality of the projected image suggests the feature will be robust against deviations from accurate replication arising during production.

### 6.3 Durability testing

The image projected by the PBI is easily observed by the user. However, the PBI only has value as a security feature if it retains efficacy in circulation. A targeted set of tests, considered most likely to reduce the efficacy of the PBI, were conducted on opacified material from a print trial. Previous testing has established that the UV curable resin used to produce the feature is robust in circulation.

The standard crumple test was considered most likely to reduce the efficacy of the feature, and reflects a common mode of damage for banknotes in circulation. Samples were subjected to eight repetitions of a standard crumple test; a durability threshold also used for overt features such as diffractive foils. The progression of efficacy over increasing crumples is shown in Figure 13. It can be seen that the efficacy of the PBI drops away sharply after enduring more than six crumples.

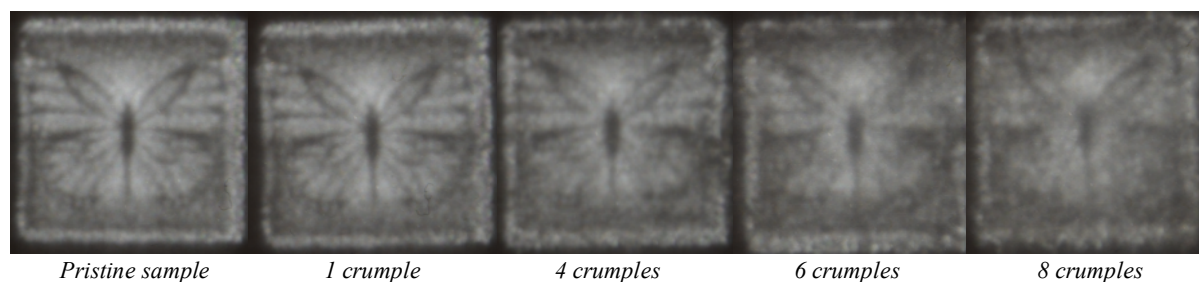


*Figure 13: Progression of wear of the PBI feature in a standard crumple test; the quality of the projected image deteriorates as more repetitions of the test are performed.*

While this result is not satisfactory, it is expected that planned improvements to the PBI will ensure that the requirements of this test are met. Firstly, this test was conducted on material that did not run at optimal production settings, resulting in small defects across the lens array and reducing the quality of the projected image. Secondly, the butterfly image chosen has shown that images containing fine lines may not be the optimal design. Further trials are being conducted testing designs containing a range of linewidths to establish design rules for the feature; this is discussed further in Section 7. In particular, setting a minimum linewidth or size for design elements will ensure the efficacy of the feature is maximised after crumpling.

The efficacy of the PBI was retained after soiling and abrasion tests.

### 6.4 Counterfeit resistance

Preliminary adversarial assessment of the PBI has determined it to have greater counterfeit resistance than similar device-assisted features, such as DOEs. The projection of the high-contrast image is a straightforward effect, easily

describable to the public. The design of the lens array ensures a complete lack of connection between the appearance of the lens array and the projected image, preventing use of primitive level counterfeiting techniques. The specialist knowledge required to produce the lens array increases the security of the feature relative to DOEs, which can be created using freely available software. Furthermore, the projected image from DOEs can be recreated by replicating only the edges of the diffractive structures, but the PBI projected image requires the entire curvature of the lens to project the image. The level of skill required to re-originate the lens array contrasts with holography-based features, which can be reproduced through commercially available equipment.

An obvious counterfeiting technique, available to the hobbyist and professional counterfeiter, is the creation of an embossing tool by casting from the original feature. This method of replication is common to all exposed lens and optically-based security feature. While an embossing tool can be created, the requirement for a counterfeiter to UV emboss onto the banknote means an extra process is required, which is considered to add significant deterrent. However, as discussed in Section 4, the adversarial resistance can be enhanced by engineering the feature such that it is covered with a protective layer to prevent contact printing. This process is also discussed in Section 7.2.

## 7. FURTHER WORK

### 7.1 Design refinement

The durability testing conducted on the butterfly image showed that the fine lines in the image degrade more quickly than larger design elements during the crumple test. A minimum linewidth or size for design elements is required to ensure any design chosen retains efficacy after crumpling. The effect of element size and linewidth on efficacy is under investigation through print trials conducted using two new lens meshes. The target image and simulated lens surfaces for the two images are shown in Figure 14.

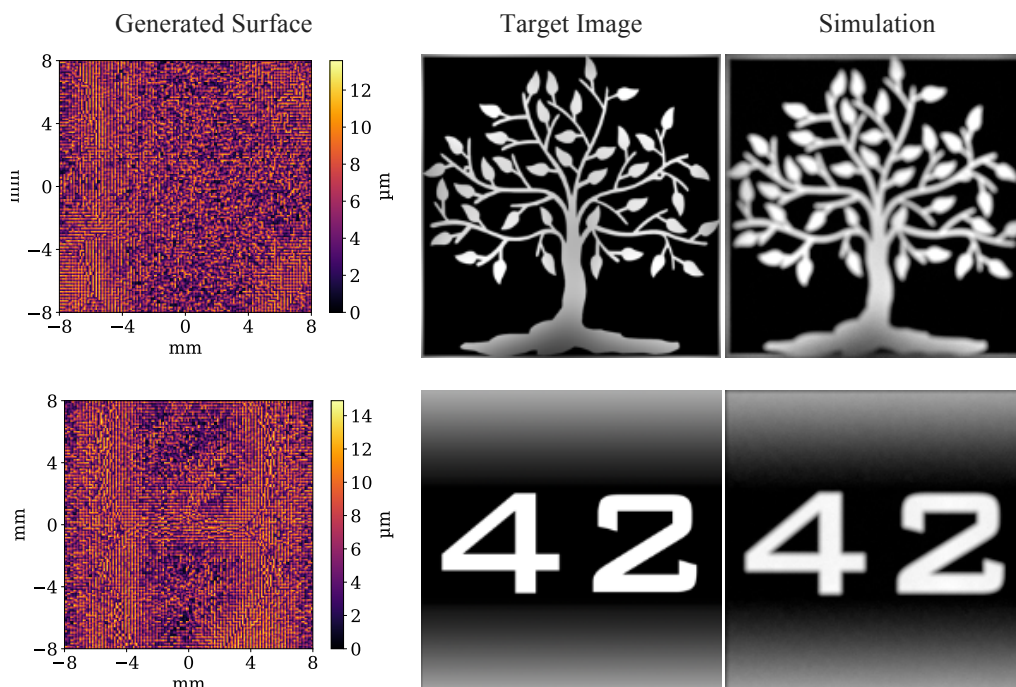
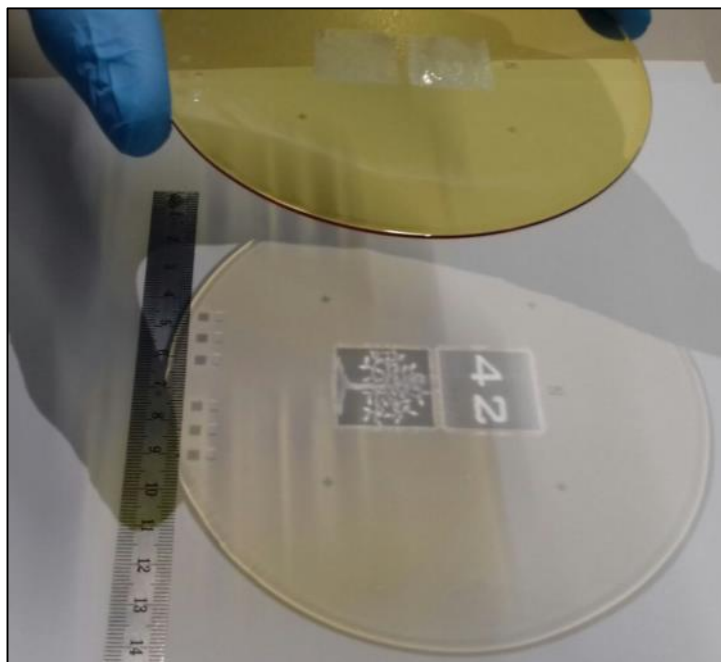


Figure 14: Simulated lens arrays and projected images for new target images

The images were chosen for two distinct reasons. The numeral image tests the opposite end of the design spectrum to the butterfly. The thick bold lines are designed to remain recognisable and robust through durability testing. The



*Figure 15: An embossing master showing images projected from new lens mesh designs*

tree design includes a number of lines of varying width, which will inform setting of a specification for minimum linewidths for use in the feature. Figure 15 shows an embossing master for these meshes, and the projected images from each array.

The tree image also presented further challenges for design of the lens mesh. The intensity of light forming different parts of the image had to be locally adjusted to ensure the thickness of the lens array remained within the  $15\ \mu\text{m}$  limit. The adjustment was performed by a custom image processing tool which divided the original image by a significantly blurred version of image. The local intensity adjustments on the target image ensure a more uniform overall light intensity distribution on the projection plane to avoid significant tilting of individual lens elements, which would also require trimming of some lens vertices to meet the thickness requirements, leading to an increase in background noise in the image

A pilot-scale reel-to-reel trial is planned for these designs. Durability testing will be conducted on the material produced.

## **7.2 High-refractive index (HRI) coatings**

Security features with exposed optical elements are considered susceptible to counterfeiters growing an embossing tool directly from the exposed structures. While this process requires some skill and specialist knowledge, and still requires the counterfeiter to enact a separate process to add the feature to counterfeits, optical elements are often coated with a protective layer to prevent any attempt at this process. However, such coatings can often substantially reduce the optical effect from the feature.

To date, all prototyping and production trials for the PBI feature have been conducted on a version of the feature where structures are exposed. However, the feature can be adapted to accommodate a protective layer. The curvature of the lens elements is inverted from convex to concave to accommodate coating with a protective layer of higher refractive index than the UV-curable resin forming the lenses.

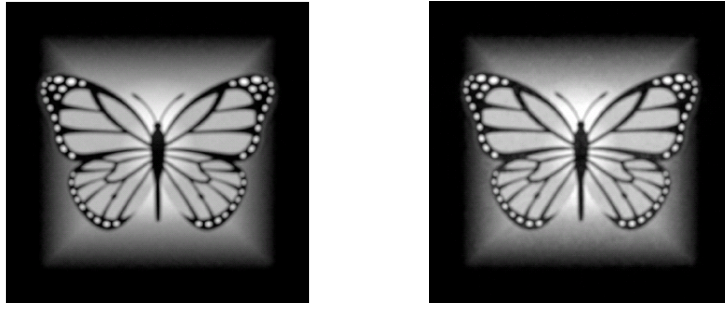


*Figure 16: Simulations of projected image from uncoated, convex lens array (left) and HRI coated, concave lens array (right).*

As noted in Section 2, the algorithm can accommodate the use of a protective coating over the lens array, creating an embodiment where the upper surface of the lens array is flat. Simulations were conducted to determine if a lens mesh could be fabricated while retaining the design constraints introduced for usability of the feature in Section 3. A high refractive index (HRI) coating of refractive index 1.7 was modelled, as this represented the highest refractive index readably accessible for banknote use. It was assumed that the HRI coating completely filled the lens structures, and also added a 3  $\mu\text{m}$  layer of consistent thickness on top of the structures.

The simulations, shown in Figure 16, demonstrated that the lens array can be designed to accommodate a HRI coating with minimal loss of clarity and contrast. The HRI version is slightly less sharp, an effect arising from the decreased refractive index differential between the HRI layer and lenses, compared to the differential between air and lenses on the original embodiment. As the refractive “power” of the lenses is lessened, the curvature and tilt of each lens element needs to be increased in order to direct light to the same area achieved for the original lenses. This effect is sufficiently large that approximately 3% of vertices need to be trimmed in order to meet the maximum height constraint of 15  $\mu\text{m}$ .

Laboratory prototypes of the lens array have been produced. HRI materials are currently being trialled with the lens array, with a focus on finding materials that could be applied at production scale.

## **8. CONCLUSION**

The PBI is a novel device-assisted banknote security feature, utilising easily accessed functionality on smartphones to provide a means of authentication that can straightforwardly be used by even untrained users. The high efficacy of the PBI arises from a ground-breaking algorithm that can generate microlens arrays capable of projecting arbitrary caustics from a diverging light source, such as a smartphone flash. The algorithm has been modified to accommodate the requirements of banknote manufacture, including limits on lens thickness. The algorithm also incorporates adversarial requirements, including the capacity to protect the exposed lens array. The PBI is considered to have strong resistance to all levels of counterfeiting.

## **9. ACKNOWLEDGEMENTS**

The Reserve Bank team would like to acknowledge the contributions of the Research & Development team to this project. In particular, Gavin Louey for conducting the durability testing, Dr Tim James for conducting profilometer measurements, and Dr Sani Muke for his consultation on adversarial analysis.

## REFERENCES

- <sup>1</sup> J. Drumm, and S. Johnson, S, *Mobile Consumer Survey 2016 – The Australian Cut*, Deloitte, <http://landing.deloitte.com.au/rs/761-IBL-328/images/tmt-mobile-consumer-2016-final-report-101116.pdf>, 2016
- <sup>2</sup> E. Gillich, H. Dorksen, and V Lohweg *Generation of Robust Optical paths – Colour Processing for Mobile Devices*, Optical Document Security conference, San Francisco, 2014
- <sup>3</sup> D. Tidmarsh, N. Sudan, “PHONEy Offers Smart Solution to Banknote Authentication”, *Currency News* **12** 2, pp 8-9, Feb 2014
- <sup>4</sup> <http://www.eyenote.gov/>
- <sup>5</sup> M. Papas, W. Jarosz., W. Jakob, S. Rusinkiewicz, W. Matusik, T. Weyrich, Goal-Based Caustics. *Computer Graphics Forum (Proc. Eurographics)* **30**, No. 2, April 2011.
- <sup>6</sup> M. Katz, *Introduction to Geometrical Optics*, World Scientific, **City** 2002
- <sup>7</sup> J. Avison, *The World of Physics*, Nelson Thornes, 2014, pg 16
- <sup>8</sup> Y. Schwartzburg, R. Testuz, A. Tagliasacchi, and Mark Pauly. High-contrast computational caustic design. *ACM Trans. Graph.* **33**, 4, 2014.
- <sup>9</sup> Y. Yue, K. Iwasaki, B. Chen, Y. Dobashi, and T. Nishita. Poisson-Based Continuous Surface Generation for Goal-Based Caustics. *ACM Trans. Graph.* **33**, 3, 2014.
- <sup>10</sup> A. Dempster, N. Laird, and D. Rubin, Maximum likelihood from incomplete data via the EM algorithm, *Journal of the Royal Statistical Society: Series B (Methodological)* **39**, 1 pp 1–38, 1977.
- <sup>11</sup> M. Balzer, T. Schloemer, and O. Deussen, Capacity-constrained point distributions: A variant of Lloyd’s method, *ACM Trans. Graph. (Proc. SIGGRAPH)* **28**, 3, 2009.
- <sup>12</sup> G.E.P. Box, M.E. Muller, A note on the generation of random normal deviates, *The Annals of Mathematical Statistics* **29**, 2, pp 610–611, 1958.
- <sup>13</sup> B. Walter, S. Zhao, N. Holzschuch, K. Bala, Single scattering in refractive media with triangle mesh boundaries. *ACM Trans. Graph. (Proc. SIGGRAPH)* **28**, 3, 2009.
- <sup>14</sup> E. Weinberger, Correlated and uncorrelated fitness landscapes and how to tell the difference, *Biological Cybernetics* **63** (5), pp 325–336, 1990.
- <sup>15</sup> L. Maguire and P. Fox, Security document with an optically variable image and method of manufacture, WO2010115235A1.
- <sup>16</sup> L. Maguire, The Non-diffractive Switching Image: A non-printed optically variable security device, Optical Document Security conference, San Francisco, 2012.
- <sup>17</sup> Y. Yue, K. Iwasaki, B. Chen, Y. Dobashi, and T. Nishita. Poisson-Based Continuous Surface Generation for Goal-Based Caustics. *ACM Trans. Graph.* **33**, 3, 2014.